International Journal of Microwave and Wireless Technologies, 2009, 1(2), 137–143. ©2009 Cambridge University Press and the European Microwave Association
doi:10.1017/S1759078709000178 Printed in the United Kingdom

GaN devices for power amplifier design

TERESA M. MARTÍN-GUERRERO[1], DAMIEN DUCATTEAU[2], CARLOS CAMACHO-PEÑALOSA[1] AND CHRISTOPHE GAQUIÈRE[2]

This paper describes some aspects of the fabrication and modeling of a GaN device to be employed in a power amplifier covering one WiMAX frequency band. The work has been carried out in the frame of the TARGET's NoE work package WiSELPAS. Details concerning the AlGaN/GaN device technology and the performed linear and nonlinear measurements are provided. Since these new devices require specific nonlinear models, a procedure for selecting an appropriate simplified nonlinear model and for extracting its parameters is discussed and evaluated. The developed nonlinear model has been experimentally tested under linear and nonlinear conditions. The agreement between experimental and model-predicted performance suggests that the described model could be useful in a preliminary power amplifier design.

Keywords: Wide-band-gap devices, AlGaN/GaN technology, Nonlinear model, Power amplifiers

Received 12 March 2005; Revised 4 May 2005; first published online 12 May 2009

I. INTRODUCTION

The Network of Excellence TARGET ('Top Amplifier Research Group in an European Team') was created with the aim of demonstrating effective collaboration among Research Groups in Europe in the frame of cutting-edge microwave and millimeter wave technologies. The Work Package named WiSELPAS ('From Semiconductors to Linearised Wireless Power Amplifiers') pursued the fabrication of different power amplifiers starting from the device fabrication [1].

One of the proposed designs was a power amplifier based on an innovative AlGaN/GaN technology. Specific devices were specially designed and fabricated, and the aim was to assess the performance of such devices in power amplifier applications. In this work the first stage of the corresponding work package, composed of a general description of both the technology and a dedicated device nonlinear model, is described. The device was manufactured and characterized by the Institut d'Electronique, de Microélectronique et de Nanotechnologie (IEMN) and the simplified nonlinear model was developed at the Universidad de Málaga (UMA).

The wide-band-gap device technology used and the measurements involved in the device characterization procedure are described in Section II. Sections III and IV are devoted to the linear device model used to develop the nonlinear one. The dedicated nonlinear model is described in Section V, and, finally, a comparison between measured and model-predicted device performance is presented in Section VI.

[1]Departamento de Ingeniería de Comunicaciones, E.T.S. Ingeniería de Telecomunicación, Universidad de Málaga, Campus de Teatinos, E-29071 Málaga, Spain. Phone: + 34 952133395; Fax: +34 952132027
[2]Dépt. Hyperfréquences et Semiconducteurs, Institut d'Electronique, de Microélectronique et de Nanotechnologie (IEMN), Université de Lille, Av. Poincaré, BP 69, F-59652 Villeneuve d'Ascq, France. Phone: + 33 (0)320197829; Fax: +33 (0)320197888.
Corresponding author:
T.M. Martín-Guerrero
E-mail: teresa@ic.uma.es

II. AVAILABLE AlGaN/GaN DEVICE TECHNOLOGY

Wide-band-gap devices are very promising candidates for high-frequency and high-power applications thanks to the high voltage and current capabilities. Nitride-based HEMTs have been fabricated since several years at TIGER, a common laboratory between III-V lab and IEMN. AlGaN/GaN prototypes for microwave power amplification are usually fabricated from epitaxial stacks on silicon carbide or silicon substrate. Single crystal semi-insulating silicon carbide (4H or 6H) is the most suitable substrate material due to its lower mismatch with GaN and very good thermal conductivity (450 W/K·m), but it is still very expensive.

A) Fabrication

The devices were processed on an AlGaN/GaN epilayer grown by III/V lab on a SiC substrate. Device fabrication starts with ohmic contacts formed by rapid thermal annealing of evaporated Ti/Al/Ni/Au. The mesa isolation is obtained from multiple He+ ions implantations. Then, different gate lengths are achieved, defined by e-beam lithography based on a bi-layer resist the lift-off becomes easier. Gate deposition was performed by e-gun evaporation of a Mo/Au bi-layer. Finally the passivation step was done using SiN/SiO2 layers.

B) Characterization

The fabricated samples ($8 \times 50 \times 0.25\ \mu m^2$) were measured under microwave probes (GSG). In order to extract the nonlinear equivalent scheme, pulsed I–V (pulse width 300 ns, period 10 μs) for several quiescent bias points were performed [$(V_{DSo}, V_{GSo}) = (0, 0), (0, -9), (15, -9)$ and $(20, -9)$ V]. Then, multi-biased pulsed S-parameters for two quiescent bias points [$(V_{DSo}, V_{GSo}) = (20, -5), (20, -6)$ V] were performed up to 20 GHz for the same pulse conditions. A brief overview of the characteristics of these samples is presented

https://doi.org/10.1017/S1759078709000178 Published online by Cambridge University Press

Table 1. GaN samples characteristics.

η	V_b (V)	$R_s + R_i$ (Ω)	*Idss* (mA/mm)	G_m (mS/mm)	V_p (V)
2	1.01	3.9	1135	231	−7.8
1.93	0.85	4.6	1120	224	−8
V_{DS} (V)	V_{GS} (V)	Mod (H21) at 10 GHz (dB)		*Ft* (GHz)	*Fmax* (GHz)
20	−6	11.2		37	86

in Table 1. Figure 1 shows MAG-MSG measured at different bias conditions.

Large signal measurements were carried out at 4 GHz using a Large Signal Network Analyser. These measurements are useful to check nonlinear model accuracy and also to validate epitaxy quality and technological steps. At 20 V the maximum output power density is equal to 4.4 and 6 W/mm with a drain source voltage of 20 and 30 V, respectively.

III. LINEAR CIRCUIT MODEL

The linear circuit model used to simulate the small-signal behavior of the device is shown in Fig. 2. The topology of this circuit is based on some preliminary simulation efforts that suggested which elements were really significant for modeling the small-signal behavior of the device.

In particular, parasitic RC branches were required to properly simulate the pinched-off measurements under 'cold' bias conditions ($V_{DS} = 0$ V). These two branches were introduced to cope with some isolation problems under dynamic conditions. Both RC branches have the same relaxation time, i.e. $\tau_p = R_{pg}C_{pg} = R_{pd}C_{pd}$. It should be mentioned that R_s and L_s have not been included in the circuit due to their small values, obtained when simulating the device under 'cold' bias conditions. Resistors R_g and R_d are considered linear elements. Therefore the extrinsic part of this linear circuit model is composed of only seven elements, namely L_g, L_d, C_{pg}, C_{pd}, τ_p, R_g, and R_d. The extrinsic element values were extracted from S-parameters using the standard procedure based on 'cold' measurements. First, the values for L_g and L_d were consistently extracted from measurements for high values of V_{GS}; next, the remaining element values were obtained by fitting the pinched-off *S*-parameters. The obtained values for these extrinsic elements are shown in Table 2.

For the intrinsic part of the device a standard quasi-static-circuit model with only six elements (C_{gs}, C_{gd}, C_{ds}, G_m, G_{ds}, and τ_m) that provides a reasonable fitting to the measured *S*-parameters was chosen. The values of these intrinsic elements are extracted from pulsed *S*-parameter measurements by an optimization routine while keeping the extrinsic element values fixed. An illustrative example of the fitting provided by this linear circuit model is shown in Fig. 3.

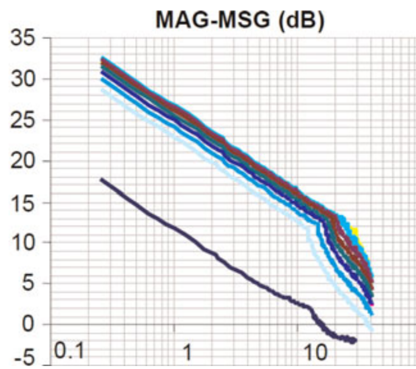

Fig. 1. Maximum stable gain and maximum available gain of the device for several bias conditions ($V_{DS} = 20$ V, V_{GS} from −9 to 0 V).

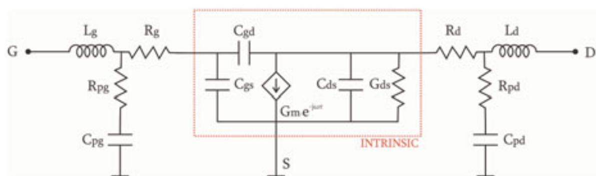

Fig. 2. Linear circuit model for simulating the small-signal behavior of the device ($\tau_p = R_{pg} \cdot C_{pg} = R_{pd} \cdot C_{pd}$).

IV. BIAS DEPENDENCE OF THE LINEAR CIRCUIT MODEL

In order to identify the main nonlinearities present in the device, the bias dependence exhibited by the intrinsic elements was investigated using the available pulsed *S*-parameter measurements for one available quiescent bias point [(V_{DSo}, V_{GSo} = (20, −5) V]. The extracted model element values as a function of bias results are shown in Fig. 4. The fitting error is almost uniform and takes reasonable values for all the points in the used bias grid. This confirms the capabilities of the proposed linear circuit model.

The bias dependence exhibited by the intrinsic elements suggests that the main nonlinearities are C_{gs}, G_m, and G_{ds}, and therefore that a simplified nonlinear circuit model, valid for the region in the I_{DS}–V_{DS} plane where the load-line will be located, could be obtained by keeping C_{gd}, C_{ds} and τ_m

Table 2. Extracted values for parasitic elements.

L_g	C_{pg}	R_g	L_d	C_{pd}	R_d	τ_p
105 pH	25 fF	1.3 Ω	104 pH	49 fF	0.8 Ω	12.5 pS

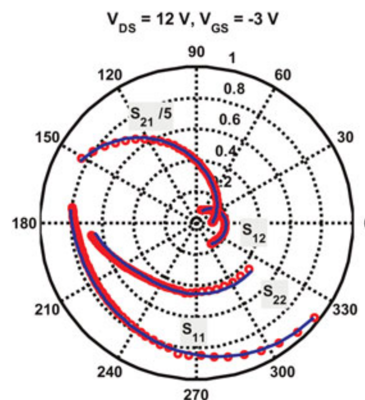

Fig. 3. Measured (o) and model-predicted (continuous line) *S*-parameters under pulsed bias conditions ($V_{DS} = 12$ V, $V_{GS} = -3$ V, from quiescent bias point $V_{DSo} = 20$ V, $V_{GSo} = -5$ V).

https://doi.org/10.1017/S1759078709000178 Published online by Cambridge University Press

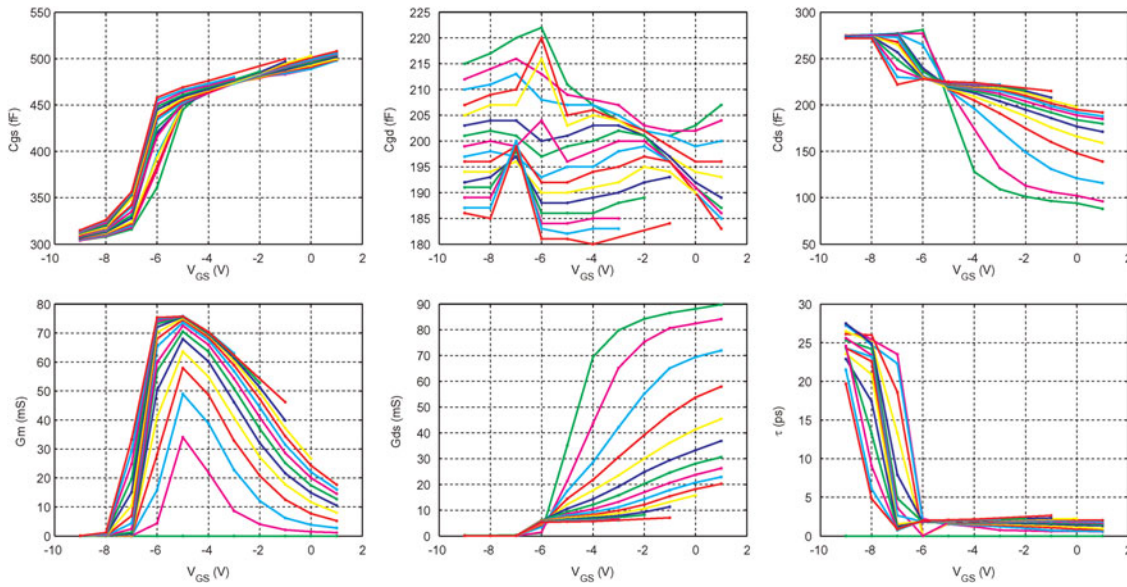

Fig. 4. Bias dependence of intrinsic small-signal model elements ($0\ \mathrm{V} < V_{DS} < 15\ \mathrm{V}$); quiescent bias point $V_{DSo} = 20\ \mathrm{V}$, $V_{GSo} = -5\ \mathrm{V}$.

bias independent. Their corresponding values were then calculated by averaging the extracted values for the V_{DS} 'window' used in the subsequent large-signal characterization ($11\ \mathrm{V} < V_{DS} < 15\ \mathrm{V}$), and they are shown in Table 3.

V. NONLINEAR CIRCUIT MODEL

After the approximations described in the previous section, the simplified nonlinear circuit model consists of only two nonlinear elements: the gate-source capacitance (C_{gs}) and the drain-source current source (I_{DS}), from which G_m and G_{ds} are derived.

A) Gate-source capacitance nonlinear model

It is clear from Fig. 4 that capacitance C_{gs} is mainly controlled by V_{GS}, since the influence of V_{DS} is very mild. This fact is used to further simplify the nonlinear model. The values for this capacitance have been calculated by averaging, for each V_{GS}, the values for different V_{DS} bias.

To model the variation of C_{gs} with V_{GS}, the C_{gs} nonlinear model proposed by Fager *et al.* [2], and already used for modelling GaN HEMTs [3, 4], was selected. This model is described by (see [4] for a detailed explanation of model parameters)

$$C_{gs}(V_{gs}) = C_1 + C_{gso}(1 + \tanh(P10 + P11 \cdot V_{gs})). \quad (1)$$

The simulation provided by this model, using the parameter values contained in Table 4, is depicted in Fig. 5.

Table 3. Final values for the 'linearized' intrinsic circuit model elements.

C_{gd}	C_{ds}	τ_m
206 fF	138 fF	1.0 pS

Table 4. Final values for C_{gso} nonlinear model parameters.

$C1$	C_{gso}	$P10$	$P11$
299 fF	95 fF	3.937	0.642 V^{-1}

B) Drain-source current (I_{DS}) nonlinear model

The parameter extraction procedure for this element is mainly based on the proper fitting of the measured small-signal transconductance in the saturation region for a representative V_{DS} value. The employed model must be able to simulate the measured 'shape' of the transconductance G_m as a function of V_{GS} (see Fig. 4). This result is consistent with that obtained by Cabral *et al.* for a different GaN HEMT [3], who pointed out the asymmetric behavior of such a variable – i.e., a sudden rise near turn-on followed by a smooth decrease toward 0 V. Therefore, and following [3], the nonlinear

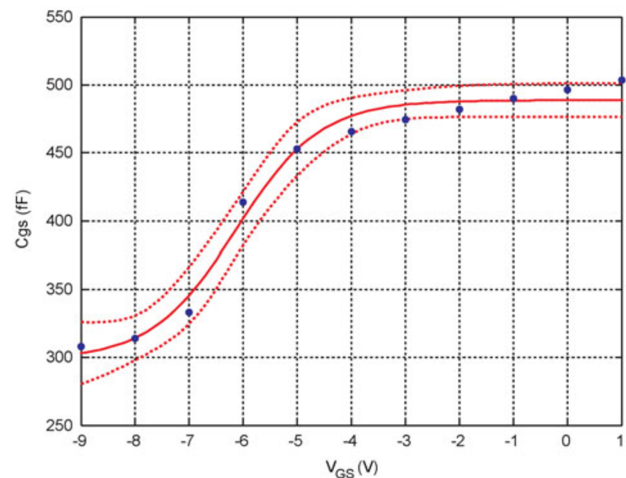

Fig. 5. Measured (•) and predicted (continuous line) $C_{gs}(V_{GS})$ values using Fager's model for capacitance. Dotted lines indicate 95% confidence prediction-bounds.

https://doi.org/10.1017/S1759078709000178 Published online by Cambridge University Press

current model proposed in [4] was adopted. Model equations, and a detailed description of their parameters, can be found in [3] and [4]. They are partly reproduced again here for the sake of completeness:

$$I_{DS}(V_{GS}, V_{DS}) = \frac{\beta V_{GS}^2}{1 + (V_{GS_3}^{plin}/V_L)}(1 + \lambda V_{DS}) \tanh\left(\frac{\alpha V_{DS}}{V_{GS_3}^{psat}}\right)$$

$$\text{with } V_{GS_3}(V_{GS_2}) = VST \ln(1 + \exp(V_{GS_2}/VST)),$$

$$V_{GS_2}(V_{GS_1}) = V_{GS_1} - \frac{1}{2}\left(V_{GS_1} + \sqrt{(V_{GS_1} - VK)^2 + \Delta^2} - \sqrt{VK^2 + \Delta^2}\right),$$

$$V_{GS_1}(V_{GS}, V_{DS}) = V_{GS} - V_T \text{ and } V_T = V_{T0} + \gamma V_{DS}. \quad (2)$$

The extraction of the parameter values of this model can be performed by fitting the measured small-signal transconductance G_m as a function of V_{GS} for a certain value of V_{DS} in the saturation region. Table 5 presents the obtained model parameter set for $V_{DS} = 12$ V where β^*, α^*, and V_T are the parameters that depend on V_{DS}. Parameters β^* and α^* are given by Equations (3) and (4) while V_T is in this case almost bias independent, i.e. $\gamma = 0$.

$$\alpha^* = \alpha \cdot V_{DS} \quad (3)$$

$$\beta^* = \beta \cdot (1 + \lambda V_{DS}). \quad (4)$$

The fitting of G_m provided by this model is shown in Fig. 6. Also shown in this figure are the higher order derivatives

$$G_{m2}(V_{GS}) = \left.\frac{\partial G_m}{\partial V_{GS}}\right|_{V_{DS}=cte} \quad (5)$$

and

$$G_{m3}(V_{GS}) = \left.\frac{\partial^2 G_m}{\partial V_{GS}^2}\right|_{V_{DS}=cte} \quad (6)$$

computed from the model. It is clear in this figure that the simulation of G_m provided by this model is rather good.

In a second step, and in order to investigate the influence of V_{DS}, the model parameters not depending on this voltage were kept fixed, and the other three were extracted for different V_{DS} values (from 10 to 15 V) by fitting the corresponding measured small-signal transconductance G_m. The obtained model parameter set is shown in Table 6.

Although the fitting provided by this model for different V_{DS} values can be considered good, it slightly deteriorates as V_{DS} separates from 12 V, the V_{DS} value used to extract the other parameters.

Table 5. Extracted parameter values for current source I_{DS} (V_{GS}, V_{DS}) for $V_{DS} = 12$ V.

β^*	V_K	V_L	V_{ST}	V_T	α^*	Δ
160 mA	5.1 V	0.69 V	0.175 V	−7.17 V	1.6	5.57 V²

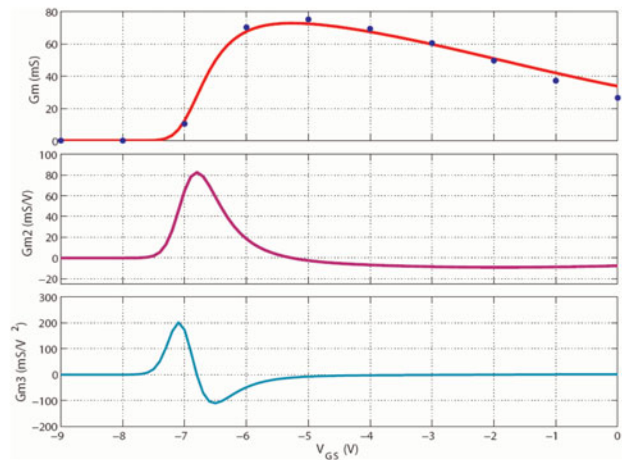

Fig. 6. Measured and modeled (•) $G_m(V_{GS})$ and model-predicted G_{m2} and G_{m3} for $V_{DS} = 12$ V as a function of V_{GS}.

Parameter values presented in Table 5 provide some interesting information concerning their dependence on V_{DS}. In particular, V_T is almost constant, which is consistent with the conclusion obtained by Cabral *et al.* [3] since they use a zero value for γ in the model. Therefore, the value obtained for $V_{DS} = 12$ V is assigned to this parameter V_T. The influence of V_{DS} on α^* is not so clear but, following the linear dependence ($\alpha^* = \alpha V_{DS}$) proposed in the model, the value $\alpha = 0.1396\ V^{-1}$ was obtained from data linear regression. The behavior of β^*, as a function of V_{DS}, almost follows the linear dependency proposed by the model. Again, a linear regression of the data yields values for β (143.1 mAV^{-2}) and λ (0.0101 V^{-1}).

VI. EVALUATION OF THE NONLINEAR CIRCUIT MODEL

Before using the nonlinear model to predict the performance of the device under nonlinear conditions, a 'tuning' of the model is required. To do that, the nonlinear model must be used in conjunction with a nonlinear simulation tool. Microwave Office has been chosen for this purpose [5]. The 'tuning' procedure is as follows. Firstly, pulsed I–V curves are used to optimize I_{DS} model parameters using the parameter values obtained in the previous section as the starting point. A comparison between measured (pulsed) and simulated I–V curves is shown in Fig. 7.

Secondly, measured pulsed *S*-parameters corresponding to the quiescent bias point to be employed for large-signal

Table 6. Extracted parameter values for drain current source I_{DS} (V_{GS}, V_{DS}) for different V_{DS} values.

V_{DS} (V)	10	11	12	13	14	15
$-V_T$(V)	7.128	7.448	7.194	7.259	7.233	7.186
$\beta^*(V_{DS})$	151.7	159.4	160.0	161.1	164.0	164.6
$\alpha^*(V_{DS})$	1.412	1.028	1.597	1.517	2.416	2.355

https://doi.org/10.1017/S1759078709000178 Published online by Cambridge University Press

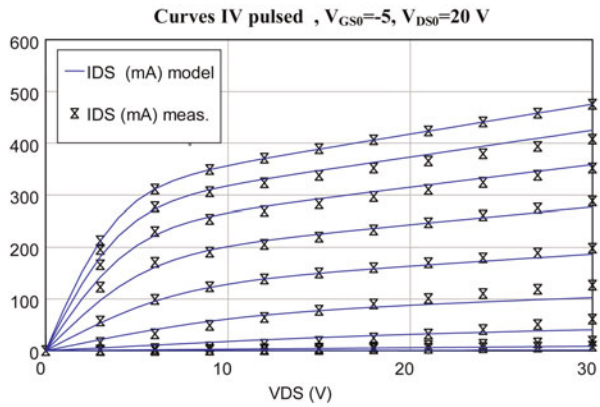

Fig. 7. Measured (pulsed) and model-predicted I_{DS} current source ($V_{GS} = -9$ to -1 V).

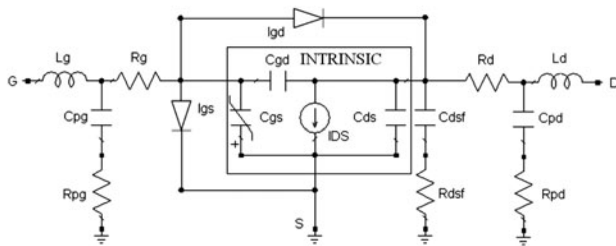

Fig. 8. Simplified nonlinear circuit model schematic.

measurements are used to calculate optimum values for the capacitance's model and to estimate the value of an added drain-source RC branch to account for some residual output conductance low-frequency dispersion.

Finally, two additional elements (diodes) are added to the gate-source and the source-drain branches to provide the model with some capability to simulate forward conduction phenomena. The resulting nonlinear model is depicted in Fig. 8. Final model parameter values can be found in [6].

This model was evaluated under both linear and nonlinear conditions. To illustrate its simulation performance under linear conditions, the measured and model-predicted small-signal power gains as a function of the frequency are depicted in Fig. 9. To illustrate its performance in the nonlinear regime,

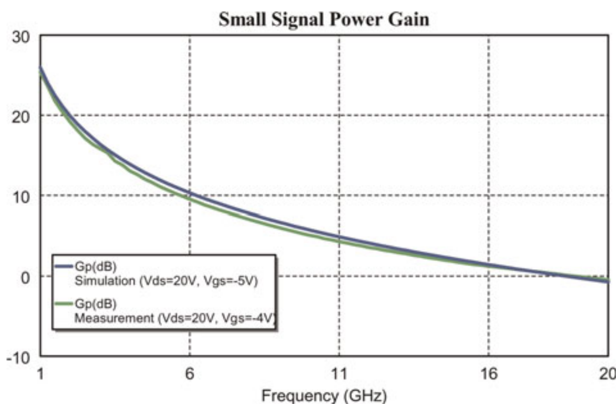

Fig. 9. Small-signal power gain measured (green) and simulated (blue) at $f_o = 4$ GHz for $V_{DS} = 20$ V, $V_{GS} = -5$ V.

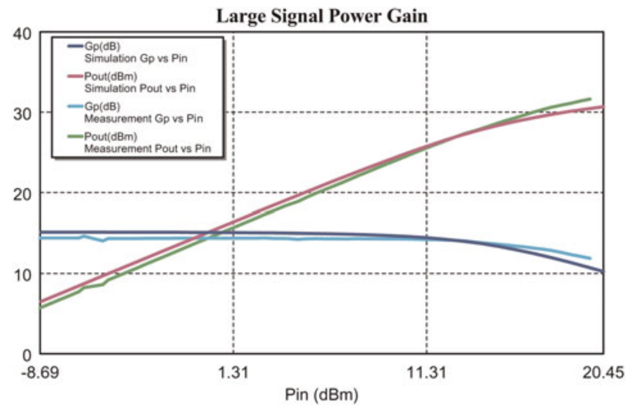

Fig. 10. Measured (cyan) and simulated (blue) gain and measured (green) and simulated (magenta) output power as a function of the source available power at $f_o = 4$ GHz for $V_{DS} = 20$ V, $V_{GS} = -5$ V.

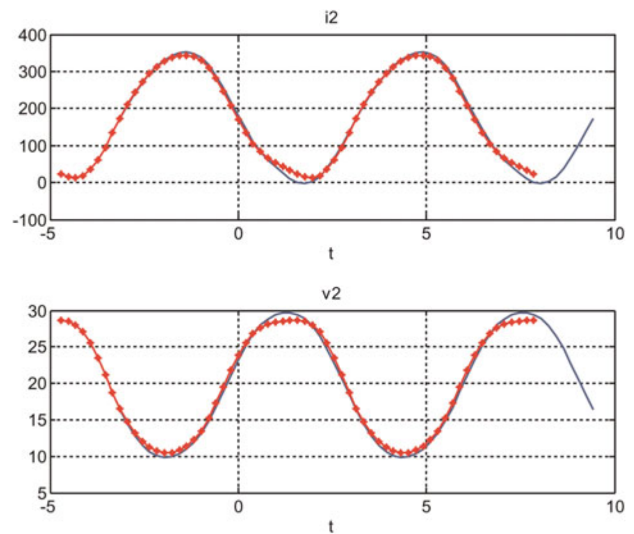

Fig. 11. Measured (*) and model-predicted (continuous line) drain current (mA) and voltage waveforms at 1 dB compresion point ($f_o = 4$ GHz, $V_{DSo} = 20$ V, $V_{GSo} = -5$ V).

the measured and model-predicted output powers as a function of the source available power when the device is loaded with $\Gamma_L = 0.193\angle 68^\circ$ at the fundamental frequency (4 GHz), and with 50 Ω at higher harmonics, are shown in Fig. 10. In addition, measured and model-predicted output waveforms for a given input power (1 dB compression point) are depicted in Fig. 11. In all cases the agreement between experimental and simulated performance is considered to be reasonably good within the limitations of the developed model.

The described model has been employed to design a low-distortion power amplifier which was manufactured and characterized. Details of this work can be found in [6].

VII. CONCLUSION

The development of a nonlinear model for a given device is not an easy task, especially if the device is a power device based on a new technology such as GaN HEMTs. The aim

https://doi.org/10.1017/S1759078709000178 Published online by Cambridge University Press

of this work wasto describe some aspects of the fabrication and nonlinear modeling of a GaN HEMT to be used in the design of a power amplifier. Some particular aspects of the modeling of such devices have been identified and taken into consideration when developing a simplified dedicated nonlinear model. Comparison between experimental and model-predicted performance, under linear and nonlinear regimes, indicates that the developed model is good enough to be employed in a preliminary power amplifier design, although self-heating phenomena have not been properly modeled.

ACKNOWLEDGEMENT

This work was partially supported by the EU network TARGET "Top Amplifier Research Group in a European Team" (IST-1-507893-NOE) and by the Junta de Andalucía (Regional Government of Andalusia, Spain) under project P07-TIC-02649.

REFERENCES

[1] Lavrador, P.M.; Pedro, J.C.: An overview of WiSeLPAs: from semiconductors to linearised power amplifiers, in Proc. TARGET DAYS – 2007, Monte Porzio Catone, Italy, December 16–17, 2007, 115–119.

[2] Fager, C.; Pedro, J.C.; Carvalho, N.B.; Zirath, H.: Prediction of IMD in LDMOS transistor amplifiers using a new large-signal model. IEEE Trans. Microw. Theory Tech., **50**(12) (2002) 2834–2842.

[3] Cabral, P.M.; Pedro, J.C.; Carvalho, N.B.: New nonlinear device model for microwave power GaN HEMTs, in IEEE MTT-S Int. Microwave Symp. Dig., Fort Worth, Texas, June 6–11, 2004, 51–54.

[4] Cabral, P.M.; Pedro, J.C.; Carvalho, N.B.: Nonlinear device model of microwave power GaN HEMTs for high power-amplifier design. IEEE Trans. Microw. Theory Tech., **52**(11) (2004) 2585–2592.

[5] Applied Wave Research, Inc. (www.mwoffice.com).

[6] Martín-Guerrero, T.M.; García, J.A.; Ng-Molina, F.Y.; Mediavilla, A.; Camacho-Peñalosa, C.; Ducatteau, D.; Gaquière, C.: Low distortion power amplifier design based on GaN monolithic device, in Proc. 11th Int. Symp. Microwave and Optical Technology (ISMOT 2007), Monte Porzio Catone, Italy, December 17–21, 2007, 365–368.

Teresa M. Martín-Guerrero was born in Málaga, Spain. She received the Licenciado en Ciencias Físicas degree (M.Sc. equivalent) from the Universidad de Granada, Granada, Spain, in 1990, and the Doctor Ingeniero de Telecomunicación degree (Ph.D. equivalent) from the Universidad de Málaga, Málaga, Spain, in 1995. Her doctoral dissertation focused on distributed effects and modeling of field-effect transistor (FET)-type devices. In 1991 she joined the Departamento de Ingeniería de Comunicaciones, Universidad de Málaga, as an Assistant Professor, and in 1999 became an Associate Professor. Her current research activities deal with microwave and millimeter-wave device modeling, and differential techniques for positioning using global satellite systems.

Damien Ducatteau was born in Linselles, France, in 1968. He received an engineering diploma from the University of Lille 1 in 1996 and a Ph.D. degree in elecronics at the Institut d'Electronique, de Microélectronique et de Nanotechnologie (IEMN) Laboratory, Villeneuve d'Ascq, France, in 2008.

In 1997, for four years, he was involved with the European Space Agency (ESA) in the ROSETTA project, during which time he developed the RF electronic part and the radar test procedures of the CONSERT instrument. In 2001, he joined the IEMN laboratory, where he was in charge of the microwave and nonlinear test characterization of HEMT AlGaN/GaN devices for the common Laboratory between IEMN and THALES III–V Labs. His research activities include the power behavior of electronic devices and he is mainly involved with nonlinear characterization at high frequencies. He is currently the Head of the technical team that has in charge the common microwave facilities of IEMN since 2006.

Carlos Camacho-Peñalosa received the Ingeniero de Telecomunicación and Doctor Ingeniero degrees from the Universidad Politécnica de Madrid, Madrid, Spain, in 1976 and 1982, respectively. From 1976 to 1989, he was with the Escuela Técnica Superior de Ingenieros (ETSI) de Telecomunicación, Universidad Politécnica de Madrid, as Research Assistant, Assistant Professor, and Associate Professor. From September 1984 to July 1985, he was a Visiting Researcher with the Department of Electronics, Chelsea College (now King's College), University of London, London, U.K. In 1989, he became a Professor with the Universidad de Málaga, Málaga, Spain. He was Director of the ETSI de Telecomunicación (1991–1993), Vice-Rector (1993–1994), and Deputy Rector (1994) of the Universidad de Málaga. From 1996 to 2004, he was the Director of the Departamento de Ingeniería de Comunicaciones, ETSI de Telecomunicación, Universidad de Málaga. From 2000 to 2003, he was Co-Head of the Nokia Mobile Communications Competence Centre, Málaga, Spain. His research interests include microwave and millimeter solid-state circuits, nonlinear systems, and applied electromagnetism. He has been responsible for several research projects on nonlinear microwave circuit analysis, microwave semiconductor device modeling, and applied electromagnetics.

Christophe Gaquière is Professor at the University of Lille and carries out his research at the Institut d'Electronique de Microélectronique et de Nanotechnology (IEMN). His topics include design, fabrication, and characterization of HEMTs and HBT devices. He works on GaAs, InP,

https://doi.org/10.1017/S1759078709000178 Published online by Cambridge University Press

metamorphic, and GaN HEMTs. His main activities are microwave characterizations (small and large signals between 1 and 220 GHz) in order to correlate microwave performances with the technological and topology parameters. Today, his activities concern the investigation of two-dimensional electronic plasmons for THz solid-state GaN-based detectors and emitters and AlGaN/GaN nanowires for microwave applications. He was responsible for the microwave characterization part of the common laboratory between Thales TRT and IEMN focus on wide-band-gap semiconductor (GaN, SiC, and Diamond) up to 2007. At the present time he has in charge the Silicon millimeter wave advanced technologies part of the common lab between ST microelectronics and IEMN. Christophe Gaquière is author/co-author of more than 40 publications and 100 publications.

https://doi.org/10.1017/S1759078709000178 Published online by Cambridge University Press